communications earth & environment

Article

A Nature Portfolio journal

https://doi.org/10.1038/s43247-025-02060-3

Waterfalls enhance regional methane emissions by enabling dissolved methane to bypass microbial oxidation

Rebecca L. Rust [1,2] ✉, Annastasia Frizzell[1,3] & John D. Kessler [1] ✉

River waters are significant sources of atmospheric methane whose local emissions increase with river slope and turbulence. However, when integrated regionally, the amount of dissolved methane released to the atmosphere is uninfluenced by local changes in turbulence when no additional loss mechanisms are present. Here we tested the hypothesis that waterfalls enhance both local and regional atmospheric methane emissions if microbial methane oxidation is significant in river waters. Rates of net atmospheric emission and net aerobic methane oxidation were measured in river waters containing waterfalls across western New York revealing that methane oxidation can diminish atmospheric emissions when turbulence is less. However, at waterfalls, 88 ± 1% of the dissolved methane supersaturation was released to the atmosphere, increasing net methane emission rates substantially beyond oxidation (0.1–16.2 × 10^6 nM d^{-1} for waterfall emission; 10–39 nM d^{-1} for oxidation), and ultimately enhancing regional methane emissions by enabling dissolved methane to bypass an oxidative sink.

Freshwater environments naturally emit significant quantities of methane (CH_4) to the atmosphere, despite lakes and rivers covering a relatively small percentage of global surface area[1]. The CH_4 emissions from all freshwater environments, including lakes, reservoirs, streams, and rivers (8–73 Tg CH_4 yr^{-1}) are a significant component of natural (220–350 Tg CH_4 yr^{-1}) and anthropogenic emissions (330–335 Tg CH_4 yr^{-1})[2]. Riverine systems release ~26.8 Tg CH_4 yr^{-1}, representing a large portion of freshwater CH_4 emissions[3].

The source of CH_4 in rivers is generally thought to arise from microbial methanogenesis in river sediments, however, geologic sources, and transport from leaking gas wells, landfills, and agriculture have all been identified (e.g., refs. 3–7). Once dissolved in river water, CH_4 has one of two fates: aerobic oxidation or emission to the atmosphere. At present, there are few published studies of aerobic CH_4 oxidation rates in river water, and these few results show that CH_4 oxidation can be either insignificant or the dominant removal mechanism (e.g., refs. 8–11). The widely variable nature of aerobic CH_4 oxidation in river waters mirrors more comprehensive datasets from seawater which similarly display CH_4 turnover times due to aerobic oxidation of several days to several decades (e.g., ref. 12). The differences in aerobic oxidation rates have been attributed, at least in part, to differences in environmental conditions, biogeochemical conditions, and measurement techniques (e.g., refs. 12–14). Aerobic CH_4 oxidation has also displayed increasing rates with increases in dissolved CH_4 concentration[15,16], suggesting that the relatively high concentrations of dissolved CH_4 in river water could support faster rates of aerobic oxidation than what has been observed in background seawater.

In addition to aerobic oxidation, supersaturated concentrations of riverine CH_4 can also be lost due to atmospheric emission, the rates of which are increased by river turbulence[17,18]. Turbulence in rivers and streams increases the surface area of water which in turn decreases the equilibration time between dissolved gases and the atmosphere, a process known as reaeration[19]. To quantify the amount of gas exchange that occurs between the atmosphere and waters due to reaeration, reaeration coefficients have been calculated. Reaeration coefficients are a rate constant with units of $time^{-1}$, characterizing this first-order equilibration process with units of moles per volume per time. (As a point of comparison, gas transfer velocities have units of distance per time and characterize gas flux with units of moles per area per time.) The inverse of the reaeration constant represents the turnover time for riverine CH_4 due to atmospheric emission which has been shown to range from 0.008 to 10 d[20–25]. While atmospheric emission has the potential to be a larger sink of CH_4 than oxidation in riverine systems, this comparison of turnover times highlights that relatively fast rates of oxidation can indeed act as a biofilter, removing significant quantities of CH_4 that would otherwise be emitted to the atmosphere. This comparison further suggests that in regions of heightened turbulence, atmospheric emission can

[1]Department of Earth and Environmental Science, University of Rochester, Rochester, NY, USA. [2]Department of Earth, Ocean and Atmospheric Sciences, University of British Columbia, Vancouver, BC, Canada. [3]Department of BETA Sciences, Vrije Universiteit Amsterdam, Amsterdam, Netherlands.
✉e-mail: rrust2@u.rochester.edu; john.kessler@rochester.edu

overwhelm microbial oxidation and other CH_4 loss mechanisms from river water.

Few studies have examined how turbulence affects CH_4 emission in freshwater environments, and studies examining waterfalls specifically are limited. Steps, features that generally cause disruptions of flow in rivers and streams, have been investigated for their ability to enhance dissolved gas exchange with the atmosphere[19,26–28]. However, only one previous study has quantified CH_4 emission rates from waterfalls, with other greenhouse gases like CO_2 receiving more attention to date. Natchimuthu et al.[29] examined how gas emission changed with stream slope, finding that waterfalls have larger emissions of CH_4 and CO_2 compared to regions of streams with lower slopes. Previous research has established that natural waterfalls, and similar artificial structures, act as emission points for CO_2. Leibowitz et al.[30] studied waterfalls as sources of CO_2 to the atmosphere in the Preto River in Brazil and found 41%, 14.2%, and 19% decreases in pCO_2 between sites above and below three waterfalls on the Preto River. The decreases in pCO_2 were attributed to the agitation produced by the waterfalls.

Other studies have examined the effect of artificial dams and turbines on CO_2 concentrations[31–34]. These anthropogenic structures also produce agitation in river water, thus acting similarly to waterfalls to increase the river water surface area and decrease the time for the water and atmosphere to reach equilibrium. Kemenes et al.[33] found CO_2 degassing at the Balbina dam in Brazil due to turbulence leads to 51% of the annual emissions below the dam. Similarly, CH_4 emissions from dams have also been explored. Galy-Lacaux et al.[32] performed experiments to examine how dams alter net CH_4 emissions at the Petit-Saut dam in French Guiana. The dam was reported to cause a release of 80-90% of the dissolved CH_4 as water masses flowed over the dam. Work by Harrison et al.[31] modeled the CO_2 and CH_4 fluxes from reservoirs globally, and found up to half of the CH_4 lost from these structures to be attributed to degassing, with particularly high emission to the atmosphere in the tropics and subtropics.

While prior research has established that waterfalls and dams are local emissions points of CO_2 and CH_4, no previous studies have examined how waterfalls impact the relationship between the CH_4 loss mechanisms of emission and oxidation in rivers and streams. This interplay particularly impacts emissions more regionally and is best illustrated when comparing two endmember cases. In one endmember where a river system displays negligible aerobic CH_4 oxidation in river water, waterfalls will enhance local emission rates, however, cumulative emissions integrated across the regional river system remain uninfluenced. The increased emissions at the waterfall result in decreases in dissolved CH_4 concentrations and emission rates downstream, counterbalancing the waterfall enhancement (Fig. 1). By analogy, stirring a carbonated beverage will not influence the total amount of CO_2 released to the atmosphere, only the instantaneous emission rate. In the other endmember where a river system displays significant aerobic CH_4 oxidation in river water, background (non-waterfall) atmospheric emission of CH_4 is reduced. However, when a waterfall is encountered, dissolved CH_4 that would have otherwise been oxidized is released to the atmosphere, enhancing emissions compared to a river system without a waterfall. And since CH_4 oxidation rate is proportional to the dissolved CH_4 concentration, decreases in dissolved CH_4 downstream of the waterfall result in further reductions of CH_4 oxidation until the dissolved CH_4 concentration recovers (Fig. 1).

The study presented here tested the hypothesis that waterfalls, regions of most significant riverine turbulence, enhance rates of atmospheric emission of CH_4 from rivers thus enabling dissolved CH_4 to effectively bypass microbial oxidation and enhance regional as well as local CH_4 emissions. Since the validity of this hypothesis is dependent on rates of net aerobic CH_4 oxidation and net CH_4 emissions from river water, these were

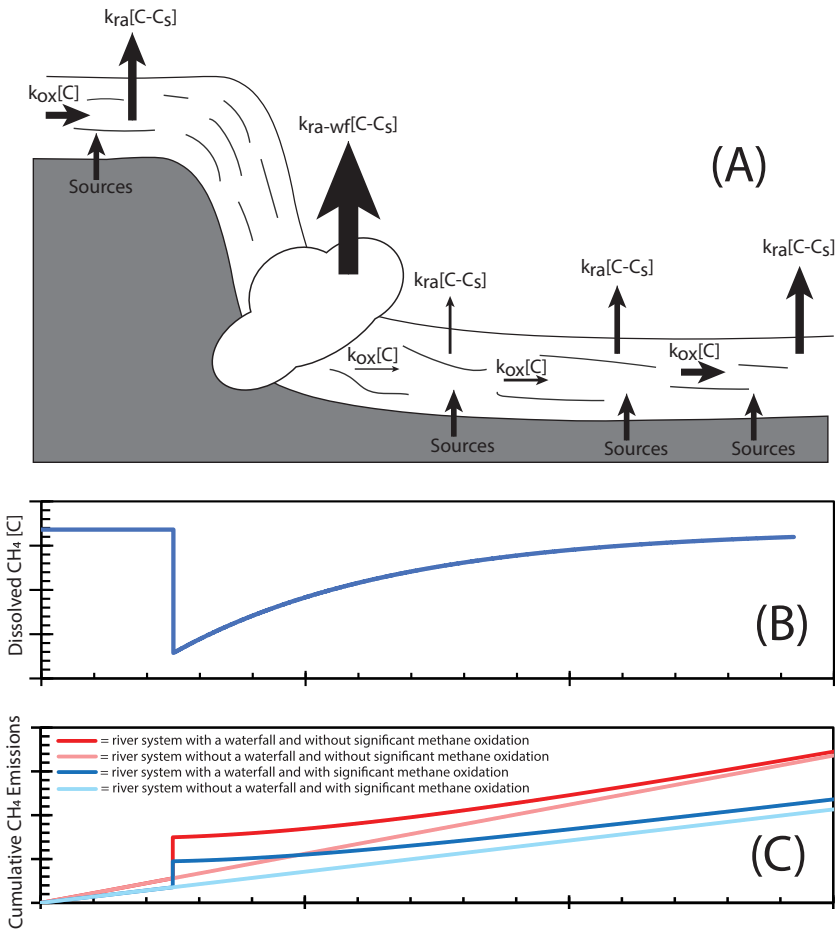

Fig. 1 | The impact of waterfalls on CH_4 emissions from rivers. A Schematic of CH_4 sources and sinks in a river containing a waterfall. $k_{ra}[C-C_s]$ is atmospheric emission, $k_{ra-wf}[C-C_s]$ is atmospheric emission at a waterfall, $k_{ox}[C]$ is aerobic oxidation in river water, *Sources* is the cumulative source of CH_4 to river water, $[C]$ is the dissolved CH_4 concentration, and $[C_s]$ is the dissolved CH_4 concentration when in equilibrium with the atmosphere. **B** Dissolved concentration of CH_4 in river water. **C** Cumulative CH_4 emission to the atmosphere. The darker and lighter hues represent rivers with and without a waterfall, respectively. The blue and red colors display rivers with and without aerobic CH_4 oxidation in the water, respectively. Both (**B**) and (**C**) are plotted as a function of distance downriver relative to the schematic in (**A**).

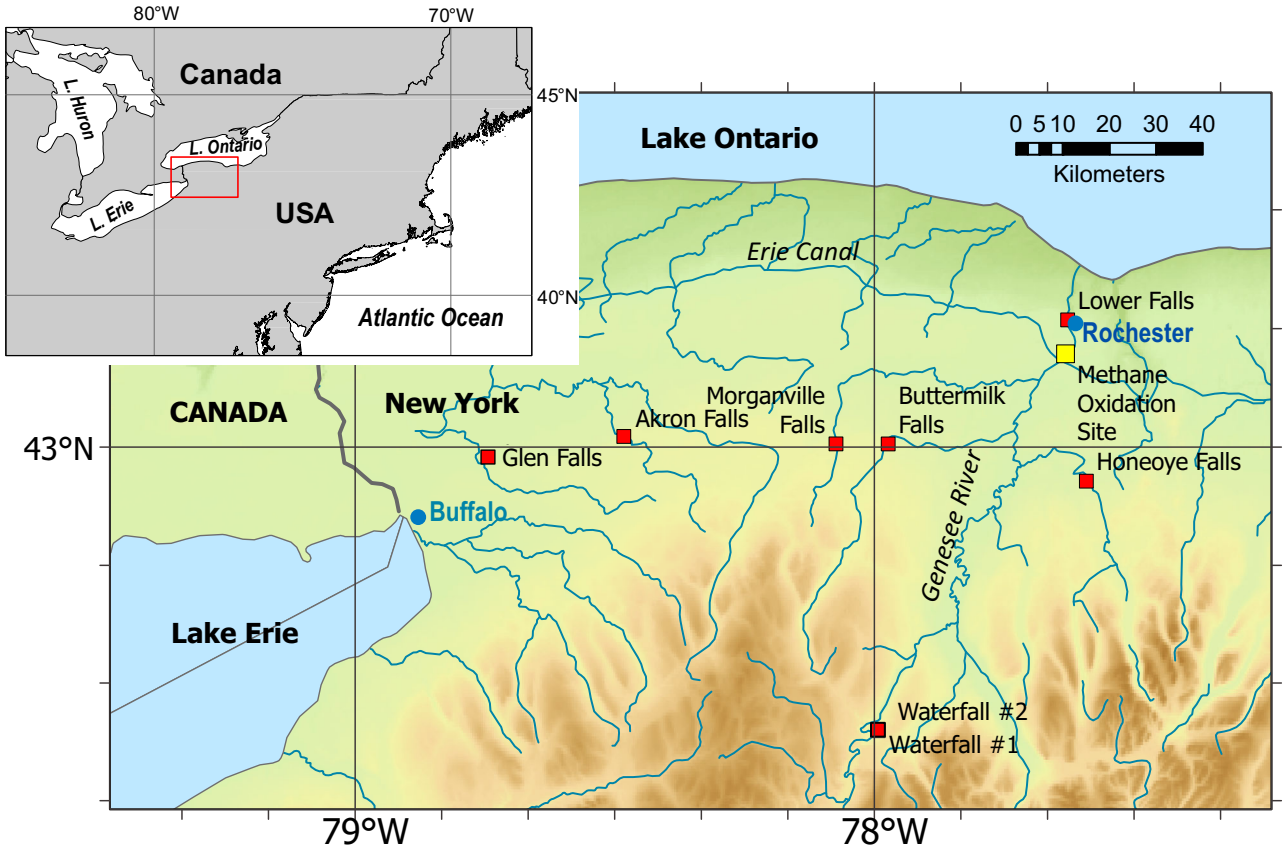

Fig. 2 | A map of the field sites where measurements were conducted. The red square symbols represent waterfalls sampled in this study. Note: Akron Falls contains two waterfalls. The yellow square represents the site of the methane oxidation study.

Table 1 | Emission characteristics for nine waterfalls measured across Western New York

Waterfall	Height (m)	Average Streamflow Rate During Sampling Period (Annual) ($m^3\ s^{-1}$)[56]	Temp (°C)	CH_4 Concentration above Waterfall (nmol L^{-1})	Change in CH_4 (nmol L^{-1})	Emission Rate ($\times 10^6$ nM d^{-1})
Lower	25.60	69.8 (70.3)	16.92	5.64	2.2	0.1
Waterfall #1	1.55		9.21	13.85	8.8	1.4
Waterfall #2	1.37		9.63	13.60	8.7	1.4
Honeoye	6.10	5.26 (3.83)	0.50	73.20	60.2	4.7
Buttermilk	18.29		0.80	11.07	5.5	0.2
Morganville	8.23		1.61	60.49	49.1	3.3
Akron (Upper)	6.10		0.29	242.64	209.2	16.2
Akron (Lower)	15.24		0.35	32.63	24.4	1.2
Glen	8.23	6.10 (4.99)	0.67	32.84	24.7	1.6

the primary measurements of this study determined in rivers and streams across Western New York containing waterfalls.

Results

To constrain how riverine CH_4 emissions are influenced by waterfalls and aerobic oxidation, waterfall CH_4 emissions were measured at nine sites across Western New York. At each waterfall, measurements of the dissolved partial pressure of CH_4 and water temperature were conducted in the field as close to the top and bottom of these waterfalls as was safely accessible. In addition, rates of net aerobic CH_4 oxidation were measured using water collected from the Genessee River at a site connecting all nine waterfalls measured during this study (see Fig. 2 and "Site Description" in the "Methods" section below for more information).

Concentration changes between upper and lower regions of waterfalls

A pattern of emission was seen at all sites, where the dissolved CH_4 concentrations were observed to be lower at the bottom of the falls than the top, establishing waterfalls as local sources of CH_4 emission to the atmosphere (Table 1). The change in dissolved CH_4 concentration from the upper to lower fall regions ranged from 2.2 to 233.6 nmol L^{-1}, with the lower bound representing Lower Falls and the upper bound representing Akron Falls. While Akron Falls contains a cascade of two waterfalls, we highlight that even the first waterfall at Akron Falls emitted 209.2 nmol L^{-1} of CH_4 (Table 1). These results support previous investigations that found CO_2 is emitted from waterfalls[29,30]. Overall, the turbulence caused by waterfalls created local emission points of CH_4 to the atmosphere.

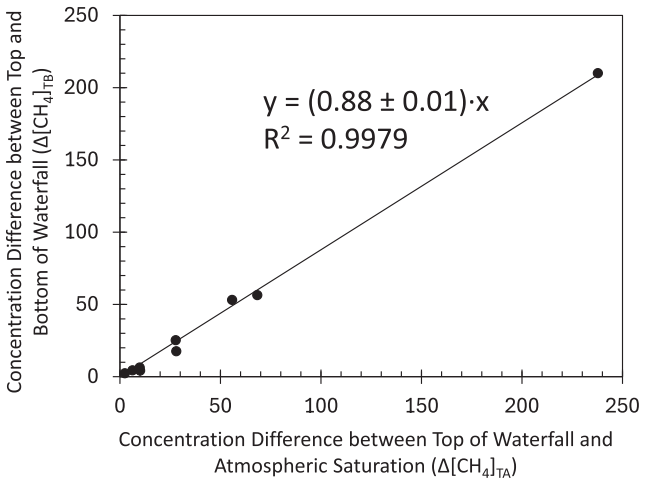

Fig. 3 | Linear relationship between $\Delta[CH_4]_{TA}$ and $\Delta[CH_4]_{TB}$ used to determine % emission from waterfalls. A strong linear correlation is found between $\Delta[CH_4]_{TA}$ and $\Delta[CH_4]_{TB}$ whose slope is equal to the fractional emission of supersaturated concentrations of dissolved CH_4 during waterfall decent. Since $\Delta[CH_4]_{TA}$ and $\Delta[CH_4]_{TB}$ are highly correlated ($R^2 = 0.9979$) with a constant slope with minimal uncertainty, variables such as waterfall height and streamflow rate do not influence the % Emission over the ranges investigated in this study.

The CH_4 emission efficiency of each waterfall was quantified by the percent of the supersaturated CH_4 concentration that was lost as water masses moved over the waterfalls. 100% emission was defined as the bottom of the falls displaying dissolved CH_4 concentrations that were in equilibrium with the atmosphere (Table 1; Eq. 1).

$$\%Emission = \frac{\Delta[CH_4]_{TB}}{\Delta[CH_4]_{TA}} \times 100 \quad (1)$$

Here, $\Delta[CH_4]_{TB}$ is the change in dissolved CH_4 concentration between the top and bottom of the waterfall. And $\Delta[CH_4]_{TA}$ is the change in the dissolved CH_4 concentration between the top of the waterfall and atmospheric equilibrium, assuming an atmospheric concentration of 1.922 ppm. Of the three parameters used in the determination of % Emission ($[CH_4]$—top, bottom, and atmospheric equilibrium), $[CH_4]_{bottom}$ likely has the largest relative uncertainty due to its concentration being near atmospheric equilibrium and unknown influences from microbubbles[18] and sediment sources of CH_4 at the point of sampling near the splashdown pool. Because of this, the determination of % Emission will have disproportionately large uncertainty when the measured value for $[CH_4]_{top}$ is closest to $[CH_4]_{bottom}$. Thus, to avoid this disproportionality and more uniformly consider the absolute uncertainty in $[CH_4]_{bottom}$, we instead calculated % Emission as the slope of the line relating $\Delta[CH_4]_{TA}$ and $\Delta[CH_4]_{TB}$ determined via linear-least squares. Doing so fits a linear regression to the data by minimizing the absolute difference between $\Delta[CH_4]_{TB}$ (i.e., the parameter that contains the largest source of relative uncertainty—$[CH_4]_{bottom}$) and the regression line (Eq. 2; Fig. 3).

$$\Delta[CH_4]_{TB} = \frac{\%Emission}{100}\Delta[CH_4]_{TA} \quad (2)$$

This analysis revealed that % Emission is 88 ± 1 % and is constant across all waterfalls investigated in this study despite changes in streamflow rate (5.26–69.8 $m^3\ s^{-1}$) and waterfall height (1.37–25.6 m) (Table 1; Fig. 3). This constant percent emission was surprising to us, especially in the case of waterfall height, as we expected the longer drop times associated with higher waterfalls to promote a greater % Emission. While this expectation is logical, this result instead reveals that even the smallest waterfall investigated here (1.37 m) provided enough drop time to promote a seemingly maximum amount of % Emission for these environmental conditions; any additional drop time beyond that produced from 1.37 m does not produce additional CH_4 emissions for the locations investigated here.

Emission rates from waterfalls

The emission rate of dissolved CH_4 from river and stream water to the atmosphere follows a first-order decay process. The supersaturated concentration of dissolved CH_4 decays exponentially to the saturated concentration, i.e., the concentration when river water is in equilibrium with the atmosphere, at a rate determined by the reaeration coefficient (Eq. 3).

$$\frac{dC}{dt} = -k_{ra}[C - C_s] \quad (3)$$

Here, C is the measured concentration of dissolved CH_4 in a river system (mol L^{-1}), C_s is the saturated concentration of dissolved CH_4 (mol L^{-1}), and k_{ra} is the reaeration coefficient (s^{-1})[35]. For the investigation conducted here, the inverse of the reaeration coefficient ($1/k_{ra}$, s) determines the residence time (τ) of CH_4 in river water as only influenced by atmospheric emission. Reported here are average net CH_4 emission rates (nM d^{-1}) at all waterfalls investigated, which is defined as $\Delta[CH_4]_{TB}$ divided by the time for water to travel from the top to the bottom of the waterfall (Table 1). However, to account for uncertainties in $[CH_4]_{Bottom}$, $\Delta[CH_4]_{TB}$ is determined using Eq. 2 ($\Delta[CH_4]_{TB} = 0.88 \times \Delta[CH_4]_{TA}$). Additionally, the more fundamental reaeration coefficient (k_{ra-wf}) and residence time (τ_{wf}) are also determined here since the average emission rate is proportional to dissolved concentration (Eq. 3), which can vary across river systems. The reaeration coefficient and residence time further enable a more normalized comparison across different waterfalls and between different processes (e.g., between emission at waterfalls vs. aerobic oxidation).

The waterfall reaeration coefficient (k_{ra-wf}) was only determined at the shortest waterfall since our % Emission analysis determined that 1.37 m provided enough drop time to promote a seemingly maximum amount of % Emission for these environmental conditions. Since it is unknown at what height less than 1.37 m produces the maximum amount of % Emission, we report the lower bound for k_{ra-wf}. The waterfall reaeration coefficient (k_{ra-wf}) was determined using the integrated version of Eq. 3, where the slope of $ln[C - C_s]$ versus time (t) is equal to the negative of the reaeration coefficient (Eq. 4). Additional details for this determination can be found in Supplementary Information Note 3.

$$ln[C - C_s] = -k_{ra}t + ln[C_0 - C_s] \quad (4)$$

C_0 in Eq. 4 is equal to the dissolved CH_4 concentration before encountering the waterfall system and $ln[C_0 - C_s]$ is equal to the y-intercept for the plot of $ln[C - C_s]$ versus t. The time for water to travel from the top to bottom of the waterfall (t) is estimated assuming free fall and incorporating the waterfall height and the acceleration due to gravity; this is likely an underestimate since water parcels and droplets will likely follow a more tortuous path during waterfall decent, thereby decreasing the reaeration coefficient and increasing the residence time. For the 1.37 m waterfall investigated here, k_{ra-wf} was determined to be 1.94 s^{-1} for CH_4. This translates to a residence time for CH_4 at waterfalls (τ_{wf}) of at most 0.51 s. Comparing the reaeration coefficients and associated residence times determined here for waterfalls against what was previously determined for river and stream systems highlights the rapid equilibration times caused by waterfalls. Outside of waterfall systems, reaeration times for rivers and streams range from 0.1 to 131.3 d^{-1} [23,24,35] resulting in residence times of 0.008–10 d or 660–864,000 s, which is 1400–1,700,000 times longer than what is caused by waterfalls.

Net methane oxidation

All incubation experiments used to assess net CH_4 oxidation displayed steadily decreasing concentrations of dissolved CH_4 as a function of time

Table 2 | Results from the net CH_4 oxidation rate experiments

Collection Date	Incubation Temperature (°C)	Light (Y/N)	Starting [CH_4] (nM)	Net CH_4 Oxidation Rate (nM d^{-1})	Net Oxidation Rate Constant (k_{ox}; day^{-1})	Turnover Time (τ_{ox}; day)
3 October 2022	13 °C	Y	332	39 ± 4	0.12 ± 0.01	8.50 ± 0.9
26 February 2023	13°C	Y	305	18 ± 2	0.059 ± 0.007	16.9 ± 2.1
26 February 2023	5 °C	N	373	10 ± 1	0.027 ± 0.004	37.3 ± 5.6
Average			337	22 ± 15	0.07 ± 0.05	21 ± 15

(Fig. 6). Similar to atmospheric emission, the loss rate of dissolved CH_4 due to aerobic oxidation follows a first-order decay process[15,36]. The concentration of dissolved CH_4 decays exponentially with time at a rate determined by the oxidation rate coefficient (Eq. 5).

$$\frac{dC}{dt} = -k_{ox}[C] \tag{5}$$

Here, C is the measured concentration of dissolved CH_4 in a river system (mol L^{-1}) and k_{ox} is the oxidation rate coefficient (d^{-1})[15]. The inverse of the oxidation rate coefficient ($1/k_{ox}$, d) determines the residence time of CH_4 in the river water with respect to aerobic methanotrophy (τ_{ox}). The oxidation rate coefficients were determined for the experiments conducted here using the integrated version of Eq. 5, where the slope of *ln[C]* versus time (t) is equal to the negative of the oxidation rate coefficient (Eq. 6).

$$ln[C] = -k_{ox}t + ln[C_0] \tag{6}$$

C_0 in Eq. 6 is equal to the dissolved CH_4 concentration at the start of the incubation and $ln[C_0]$ is equal to the y-intercept for the plot of *ln[C]* versus *t*. Further details for these calculations are provided in Supplementary Information Note 3.

The net CH_4 oxidation rate measurements conducted here covered two different seasons, fall and winter, and two different water temperatures (13 °C and 5 °C) (Table 2). The oxidation rate coefficient (k_{ox}) was the highest, and the turnover time (τ_{ox}) was the fastest, for net CH_4 oxidation determined in river water collected in October and incubated at 13 °C ($k_{ox} = 0.12 d^{-1}$; $\tau_{ox} = 8.50$d). Conversely, the oxidation rate coefficient was the lowest, and the turnover time was the longest, for net CH_4 oxidation determined in river water collected in February and incubated at 5 °C ($k_{ox} = 0.03 d^{-1}$; $\tau_{ox} = 37.31$d). We highlight that the February 5 °C incubation was conducted in the dark while the other oxidation rate experiments were subject to artificial light for 12 h per day to promote aerobic methanogenesis that may be associated with photosynthetic activity. The presence of light, and thus potentially enhanced aerobic methanogenesis would result in a decrease in the determination of net CH_4 oxidation rates, and yet the experiment containing no light reported the lowest net oxidation rate constant. This observation likely displays the more significant influence of temperature decreasing the rate constant of net CH_4 oxidation as opposed to the absence of light decreasing aerobic methanogenesis. Nonetheless, despite seasonal and temperature changes in the oxidation rate coefficient and turnover time, a general observation is that all measurements of net CH_4 oxidation are at the upper end of prior measurements of CH_4 oxidation measured in different global water reservoirs (e.g., ref. 8–10,12,15,36,37). This observation is underscored by the fact that most previous measurements of CH_4 oxidation report gross oxidation rates as opposed to the net oxidation rates reported here (see "Measurements of Net Methane Oxidation").

Discussion

The measured results presented here reveal unique characteristics of riverine CH_4 dynamics when CH_4 sources are compared to the CH_4 sinks of oxidation and atmospheric emission under both steady-state and non-steady-state conditions (Eq. 7)

$$\frac{d[C]}{dt} = Sources - k_{ox}[C] - k_{ra}[C - C_s] \tag{7}$$

The short-term losses reported in the present study agree with previous studies that observed similar net emissions of CH_4 and CO_2 at waterfalls and dams[30,32–34,38]. Previous work by Leibowitz et al.[30] suggested that the height of waterfalls may affect how much dissolved gas is emitted to the atmosphere. This was not observed for the waterfalls sampled here, which ranged in height from 1.37 to 25.60 m (Fig. 3). Rather, the percent emission remained constant (88 ± 1%) and thus the magnitude of the CH_4 mass emitted by waterfalls was controlled by the CH_4 concentration at the top of each waterfall (Fig. 3). Excluding the significant, short-term losses associated with waterfalls, riverine dissolved CH_4 concentrations trend toward a steady state where sources of CH_4 are balanced by aerobic water column oxidation and atmospheric emission sinks. This highlights that aerobic oxidation in river water, as measured here, can remove up to 55% of riverine CH_4 sources. Stated more specifically, the upper bound for k_{ox} measured in this study (0.03 to 0.12 d^{-1}) is similar to the lower bound of k_{ra} for rivers and streams measured previously outside of waterfalls (0.1 to 131.3 d^{-1})[23,24,35]. This degree of oxidative loss is in general agreement with previous measurements of aerobic CH_4 oxidation in rivers[8–10].

However, the capacity for aerobic oxidation to limit atmospheric emissions of riverine CH_4 decreases with turbulence (i.e., increases in k_{ra}). In the non-steady-state condition when a parcel of river water encounters a waterfall, the water-to-air emission increases on a near instantaneous timescale. Our measurements indicate that reaeration coefficients increase from more conventional values in less turbulent waters (0.1 to 131.3 d^{-1} [23,24,35]) to 1.94 s^{-1} at a waterfall, an increase by a factor of 1000 to 2,000,000. This increase in the reaeration coefficient causes CH_4 emission to exceed the source rate to an extent that the dissolved concentration drops, approaching atmospheric equilibrium at the bottom of the waterfall (Figs. 1, 4A, S1, and S3). If aerobic CH_4 oxidation (k_{ox}) in river water is small relative to non-waterfall atmospheric emission (k_{ra}), the effect of waterfalls would only be to compact riverine CH_4 emissions to a point source from what would naturally occur across longer spatial scales (Figs. 1, S2, and S4). However, when k_{ox} is significant compared to k_{ra}, the effect of waterfalls is to enable CH_4 to evade to the atmosphere that would have otherwise been oxidized. The concentration drop observed following waterfall emission suppresses the CH_4 oxidation sink (Eq. 5), enabling the cumulative CH_4 emission from a river system to increase above a similar river system without a waterfall (Figs. 1, 4B, S2, and S4). The degree to which CH_4 oxidation is suppressed is related to the recovery time, defined here as the time needed for the dissolved CH_4 concentration to recover to 95% of the pre-waterfall concentration (Figs. 4C, S1, and S3). However, the recovery time itself can be deceptive since longer recovery times are simply related to smaller values of k_{ra} and k_{ox}, and may not lead to enhanced CH_4 emissions if k_{ox} is small relative to k_{ra}. Only in environments where k_{ox} is significant compared to k_{ra} will waterfalls lead to an increase in cumulative CH_4 emissions across the river system more regionally. For example, when $k_{ra} = k_{ox}$, the cumulative CH_4 emissions from a riverine system increase by 31.4% when a waterfall is present (Fig. 4D).

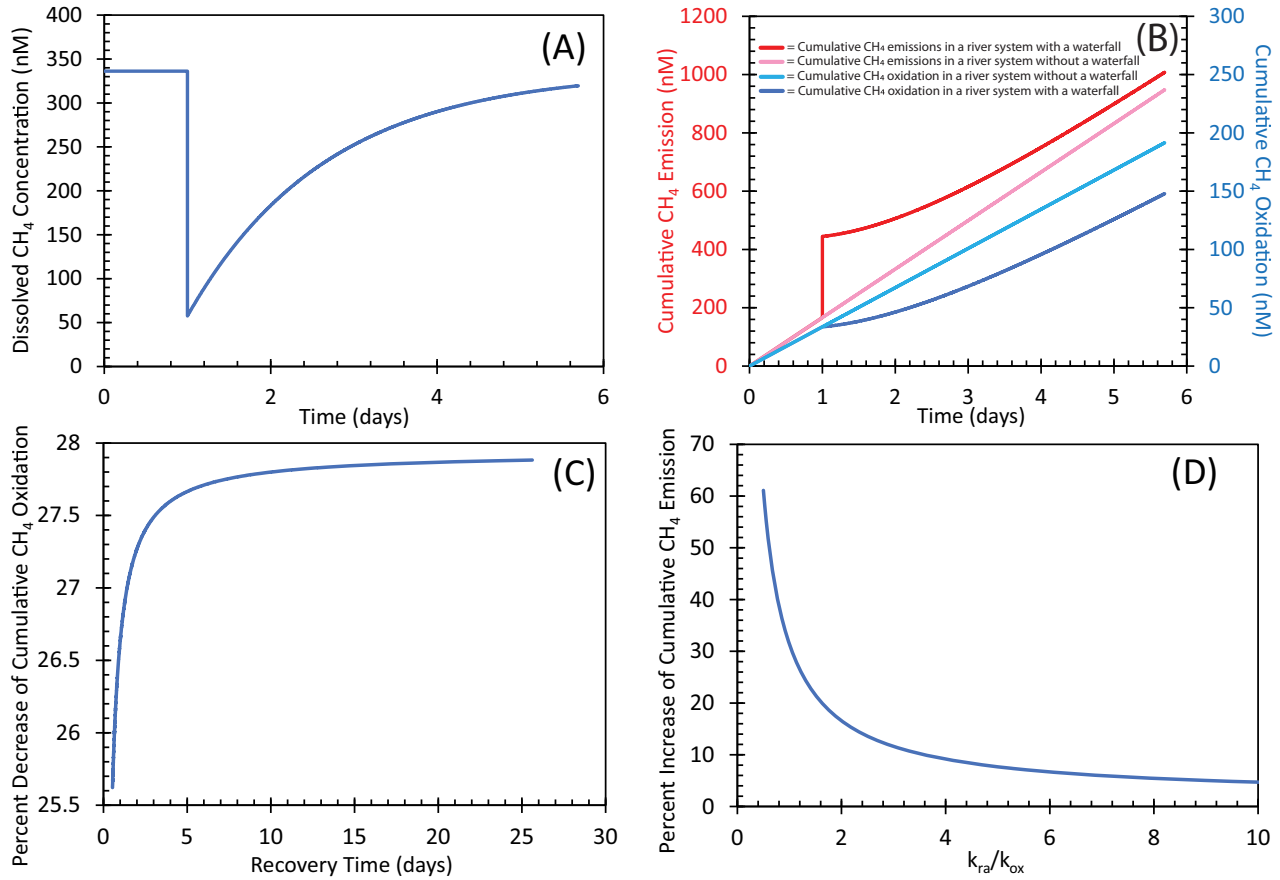

Fig. 4 | Modeled effects of waterfalls on riverine methane dynamics. Modeled riverine dissolved CH_4 concentration, cumulative atmospheric emissions, and cumulative CH_4 oxidation as a function of time or distance downriver using Eq. 7. **A**, **B** Model parameters used are $k_{ox} = 0.1d^{-1}$, $k_{ra} = 0.5d^{-1}$, $Sources = 200nMd^{-1}$, and $C_s = 3.44nM$. A waterfall is assigned to be encountered on day 1 with $k_{ra-wf} = 167616d^{-1}$ or $1.94s^{-1}$. **B** Cumulative CH_4 emissions (red) and oxidation (blue) are modeled with the lighter hues representing a river system without a waterfall. **C** The recovery time, defined here as the time for the dissolved CH_4 concentration to recover to 95% of the pre-waterfall concentration, influences the percentage decrease in cumulative CH_4 oxidation. **D** The balance between k_{ra} and k_{ox} influences the degree to which waterfalls enhance cumulative atmospheric CH_4 emissions when integrated across the river system. Further details and simulations are provided in Supplementary Information Notes 1 and 2.

Conclusion

Here we report the discovery that waterfalls not only concentrate riverine CH_4 emissions to a point source to enhance local emissions but also enhance the overall emissions of riverine CH_4 regionally if oxidation is relatively high. The CH_4 oxidation results reported here reveal that oxidation is significant and can remove up to 55% of the source of CH_4 to river water under low turbulence conditions. However, when turbulence increases, dissolved CH_4 bypasses oxidation enhancing atmospheric emissions. Our measurements at nine waterfalls across western New York revealed high reaeration coefficients driving an increase in atmospheric CH_4 emission and a decrease in dissolved CH_4 concentrations by 88 ± 1%. Interestingly, the rapid equilibration between dissolved riverine CH_4 and the atmosphere was consistent at all waterfalls investigated in this study regardless of height, suggesting that this percent emission may be useful for constraining CH_4 emissions at waterfalls and dams more universally. Nonetheless, further measurements of k_{ox}, k_{ra}, and k_{ra-wf} in background and waterfall conditions across different seasons will help to constrain the magnitude of this CH_4 emission enhancement more precisely; however, due to the magnitudes of k_{ox} and k_{ra-wf} measured here, the discovery of enhanced regional riverine CH_4 emissions due to waterfalls appears robust and significant.

Methods

Site description

Measurements of net CH_4 emissions from waterfalls were conducted between January and May 2023 at Lower Falls in Rochester, NY, two waterfalls in Letchworth State Park in Castile, NY and six other falls along the Onondaga Necklace of Waterfalls between the greater Rochester and Buffalo, NY regions (Fig. 2). Lower Falls is a 25 m waterfall on the Genesee River that flows over bedrock containing shale and sandstone[39]. The two waterfalls sampled in Letchworth State Park were unnamed and both waterfalls, which will be referred to as Waterfall #1 and Waterfall #2, sit on Dishmill Creek and feature approximately 1-meter drops. The Onondaga Necklace of Waterfalls features seven waterfalls, six of which were able to be accessed and measured (Indian Falls sits on the Onondaga Necklace of Waterfalls but is inaccessible due to steep canyon walls and a location on private property). Traveling from east to west, Honeoye Falls is a 6 m waterfall on Honeoye Creek, Buttermilk Falls is a 18 m waterfall on Oatka Creek, Morganville Falls is a 8 m waterfall on Black Creek, Akron Falls is made up of two waterfalls with the upper falls having a 6 m drop and the lower having a 15 m drop on Murder Creek, and Glen Falls is a 8 m falls on Ellicott Creek. The Onondaga Necklace of Waterfalls sits on the Onondaga Escarpment, which is a dolomite geologic formation[40].

Net rates of aerobic CH_4 oxidation were measured using water collected from the Genessee River adjacent to the University of Rochester River Campus (43.13133°N, 77.63194°W) on 3 October 2022 and 26 February 2023. This site was chosen for both scientific and logistical reasons. Scientifically, this location connects all nine waterfalls measured during this study. Lower Falls is approximately seven river kilometers downstream of this sampling site; Waterfall #1, Waterfall #2, Honeoye Falls, Buttermilk Falls, and Morganville Falls are all on primary tributaries of the Genessee

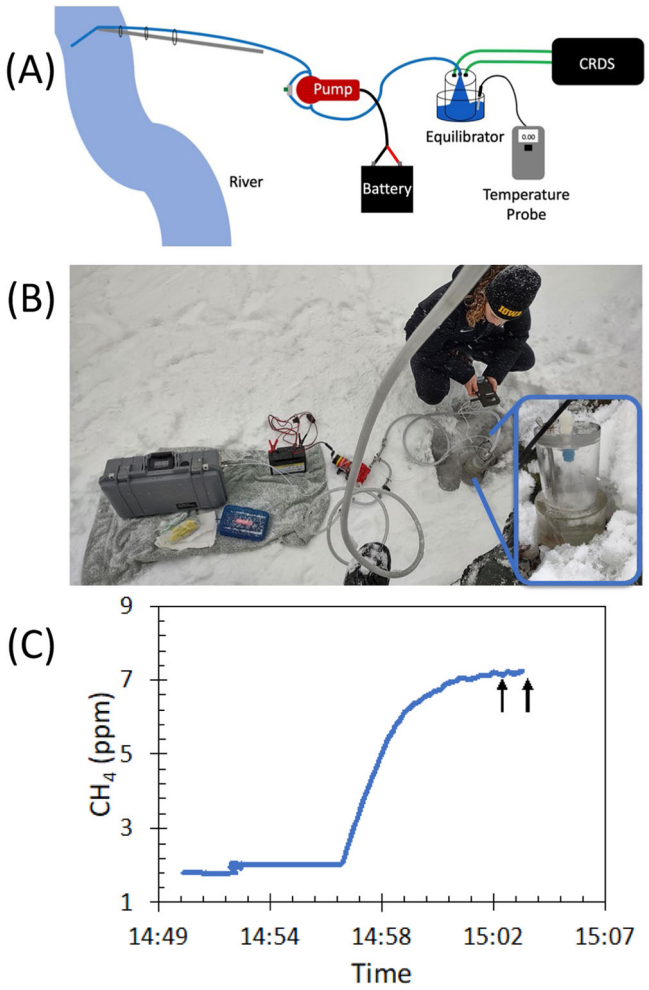

Fig. 5 | Analytical system design and data overview. Schematic diagram, photograph, and example data from the analytical system that was developed here to measure the dissolved concentration of CH_4 in river water as well as water temperature. **A** Blue lines represent tubing used for water flow, while green lines represent tubing used for air flow. **B** The blue inset features a closer view of the equilibrator designed for this research. **C** Example data displaying the equilibration time for CH_4 after measurement initiation. The black arrows surround the data points between which the average value of the dissolved gas partial pressure was calculated.

River upstream of this sampling site; and both Akron Falls and Glen Falls are on secondary tributaries of the Genessee River upstream of this sampling site (Fig. 2). Logistically, this sampling site is relatively close to the laboratory measuring the net CH_4 oxidation rates on these samples. Thus, transporting the 28 vials filled with a collective 8 L of river water back to the laboratory could be accomplished without altering the samples, damaging the equipment, or significantly taxing the investigators.

Net methane emission measurements from waterfalls

All measurements of the dissolved partial pressure of CH_4 and water temperature were conducted in the field as close to the top and bottom of these waterfalls as was safely accessible. This allowed multiple measurements to be conducted and averaged over a period of time rather than single measurements as would have occurred if discrete water samples were collected in vials. Using a field-based measurement strategy also enabled results to be determined in real-time so that adaptive sampling could occur if unexpected results were witnessed, for example, due to an inappropriate placement of the water sampling tube. Since the analytical system described below determines the partial pressure of CH_4 dissolved in water, the temperature-dependent gas solubility coefficient for CH_4 was used to translate the measured partial pressures to values of dissolved concentrations in units of moles per liter[41].

All measurements were conducted by pumping river water into an analytical system, which was designed to be portable so that the equipment could be carried to remote measurement sites either in a backpack or by hand (Fig. 5). To determine the dissolved gas concentrations, a water equilibrator was used (e.g., refs. 42–44). The equilibrator operates by enabling the dissolved gases to come into equilibrium with an isolated air headspace. Once the dissolved gases reach equilibrium with the headspace, the air headspace is measured and related to the dissolved concentrations using the gas solubility coefficient.

River water was pumped into the equilibrator using a Fimco 2.4 GPM 12 V High Performance Pump. The pump was powered by a Mighty Max 12 V 22 Ah battery that was connected to the pump via alligator clips. A pump bypass was created using 5/16-inch PVC braided tubing and a valve to control the water flow rate. Water closer to the center of the river was sampled while standing on the riverbank by connecting 5/16-inch PVC braided tubing to a 5-to-16-foot telescoping extension pole (Ettore). The sampled water was pumped directly into the equilibrator where it passed through a spray nozzle to increase the surface area of the water inside the equilibrator and promote shorter equilibration times. The equilibrator was designed so that water pooled at the bottom and then overflowed onto the riverbank while keeping an internal air headspace isolated. Inside the equilibrator, the dissolved gases reached equilibrium with the air headspace. The air headspace was connected to a LI-COR LI-7810 cavity ring-down spectrometer (CRDS) for the non-destructive analysis of CH_4 concentrations. The equilibrator headspace was connected to the CRDS using 1/8-inch firm Teflon tubing; the internal air pump on the CRDS transported equilibrator headspace gas through a water droplet trap (Pneumatic Filter AF2-213) and into the CRDS analysis cell, returning the analyzed gas back to the equilibrator in a fully closed system. Finally, an Omega HH41 temperature probe was placed in the overflow basin at the bottom of the equilibrator and the temperature value was recorded once stabilized (Fig. 5). All data was stored on the CRDS and downloaded after returning to the laboratory at the end of the sampling day.

The time required for dissolved gases to reach equilibrium with the air headspace varies based on the solubility of the gas and the design of the equilibrator[44]. For the equilibrator analytical system designed for this experiment, CH_4 took 9.5 min to reach equilibrium on average across all sites. All measurements used for final averaging were taken following the equilibration time (Fig. 5C).

Measurements of net methane oxidation

Water samples were collected from the Genesee River to assess rates of net aerobic CH_4 oxidation under the natural conditions that water masses experienced in this environment at the time of sampling. Net CH_4 oxidation, defined as the sum of aerobic methane formation and methanotrophy, was the preferred metric for this study as it determines the overall capacity of an aquatic system to oxidize CH_4 while accounting for any potential CH_4 source from aerobic methane formation. Net CH_4 oxidation was determined by incubating an array of vials filled with identical river water and sacrificing vials at regular intervals for the measurement of dissolved CH_4 concentration changes over the incubation period (Fig. 6).

River water was pumped directly into 281 mL serum vials using the same water pump, tubing, and extension pole as described previously, however, no equilibrator was attached. Water was pumped into the bottom of the vials and allowed to overflow at least five vial volumes before the sample tube was slowly removed, minimizing agitation at the water surface. All vials were sealed with sterile chlorobutyl rubber stoppers and crimp caps with care taken to not introduce bubbles during the vial filling and capping process. These stoppers were chosen as they have previously been shown not to cause toxic effects on aerobic methane oxidation[45]. The samples were then placed into an incubator equipped with a LEOTOR grow light at a yellow wavelength of 860 nm set to cycle between 12 h of light and 12 h of dark to

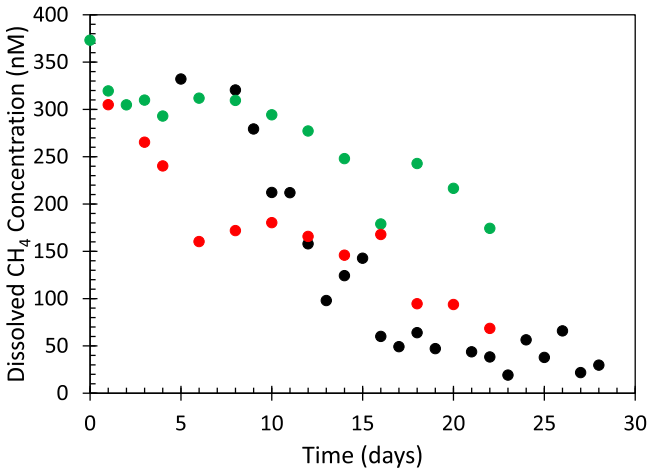

Fig. 6 | Dissolved CH_4 concentration data collected during the net CH_4 oxidation rate experiments. (Black) Samples collected in October 2022 and incubated at 13 °C. (Red) Samples collected in February 2023 and incubated at 13 °C. (Green) Samples collected in February 2023 and incubated at 5 °C. The average precision determined previously from replicate natural samples collected in different vials has a standard deviation of 5.2 % of the measured concentration[51,52].

enable aerobic methane formation that may be associated with photosynthetic activity (e.g., refs. 46–49). For the samples collected on 3 October 2022, 28 vials were filled, and the incubator was set to 13 °C to match the in-situ temperature of the Genessee River water at that time. For the samples collected on 26 February 2023, another 28 vials were filled, however, the sample vials were split with 14 samples incubated at 5 °C to match the in-situ temperature of the Genessee River water more closely at that time and the other 14 samples incubated at 13 °C to match the incubations from 3 October 2022. Additionally, the 5 °C incubation was conducted in the dark while the 13 °C incubation had the same artificial light treatment as the October experiment.

To prepare a sample for analysis at each measurement interval, a vial was sacrificed by injecting a 10 mL headspace of pure nitrogen (N_2) gas by displacing an equal volume of water; this was followed by an injection of 0.5 mL of 8 M potassium hydroxide to halt microbial activity[50]. For the October 2022 incubation, the measurement interval was once a day for 28 d, while for the February 2023 incubation, the measurement interval was once every two days with daily measurement until day four. After the N_2 gas headspace and potassium hydroxide solution were inserted, the vials were given at least 24 h for dissolved CH_4 to equilibrate with the newly injected N_2 headspace. Following this equilibration period, the headspace gas was extracted, analyzed for CH_4 concentration using an Agilent Technologies 6850 gas chromatograph with a flame ionization detector (GC-FID), and converted back to the dissolved CH_4 concentration following procedures described previously (Fig. 6)[51,52].

We chose this method because the relatively high in-situ concentration of dissolved CH_4 enabled decreases in CH_4 concentrations as a function of time to be readily quantifiable (Fig. 6). Such differences can be challenging to detect when aqueous environments are closer to atmospheric equilibrium and thus radioisotope tracers such as ^{14}C- or ^{3}H-labeled CH_4 are routinely incorporated[53]. Not involving the use of radioisotope tracers here eliminated both the nuclear regulations incurred for those experiments and the extreme potential for contaminating the natural-abundance radioisotope measurements also measured in our laboratory[54,55]. Additionally, the oxidation rate methods employed here allowed the river water to incubate in an unamended form, which is not the case for methods employing radioisotope labels[53]. Finally, no changes in CH_4 oxidation rates were observed across each month-long incubation suggesting that any potential changes in river water biogeochemistry (e.g., nutrient, dissolved O_2, or microbial community concentrations) during the incubations were insignificant at influencing these rates.

Reporting summary

Further information on research design is available in the Nature Portfolio Reporting Summary linked to this article.

Data availability

All data relevant to this investigation is found in Tables 1 and 2. These datasets as well as others relevant to this study are available at https://doi.org/10.60593/ur.d.28241174.

Code availability

All code relevant to this manuscript can be found at https://doi.org/10.60593/ur.d.28241174.

Received: 4 June 2024; Accepted: 27 January 2025;
Published online: 23 February 2025

References

1. Stanley, E. H. et al. GRiMeDB: the global river database of methane concentrations and fluxes. *Earth Syst. Sci. Data* **15**, 2879–2926 (2023).
2. Kirschke, S. et al. Three decades of global methane sources and sinks. *Nat. Geosci.* **6**, 813–823 (2013).
3. Stanley, E. H. et al. The ecology of methane in streams and rivers: patterns, controls, and global significance. *Ecol. Monogr.* **86**, 146–171 (2016).
4. Bednařík, A., Čáp, L., Maier, V. & Rulík, M. Contribution of methane benthic and atmospheric fluxes of an experimental area (Sitka Stream). *CLEAN Soil Air Water* **43**, 1136–1142 (2015).
5. Grieve, P. L. et al. Using environmental tracers and modelling to identify natural and gas well-induced emissions of methane into streams. *Appl. Geochem.* **91**, 107–121 (2018).
6. Upstill-Goddard, R. C. et al. The riverine source of CH4 and N2O from the Republic of Congo, Western Congo Basin. *Biogeosciences* **14**, 2267–2281 (2017).
7. Wendt, A. K. et al. Scientist–nonscientist teams explore methane sources in streams near oil/gas development. *Contemp. Water Res.* **164**, 80–111 (2018).
8. Bussmann, I. Distribution of methane in the Lena Delta and Buor-Khaya Bay, Russia. *Biogeosciences* **10**, 4641–4652 (2013).
9. De Angelis, M. A. & Scranton, M. I. Fate of methane in the Hudson River and Estuary. *Glob. Biogeochem. Cycles* **7**, 509–523 (1993).
10. Sawakuchi, H. O. et al. Oxidative mitigation of aquatic methane emissions in large Amazonian rivers. *Glob. Change Biol.* **22**, 1075–1085 (2016).
11. Shelley, F., Abdullahi, F., Grey, J. & Trimmer, M. Microbial methane cycling in the bed of a chalk river: oxidation has the potential to match methanogenesis enhanced by warming. *Freshw. Biol.* **60**, 150–160 (2015).
12. Mau, S., Blees, J., Helmke, E., Niemann, H. & Damm, E. Vertical distribution of methane oxidation and methanotrophic response to elevated methane concentrations in stratified waters of the Arctic fjord Storfjorden (Svalbard, Norway). *Biogeosciences* **10**, 6267–6278 (2013).
13. Pack, M. A. et al. Methane oxidation in the eastern tropical North Pacific Ocean water column. *JGR Biogeosci.* **120**, 1078–1092 (2015).
14. Shiller, A. M., Chan, E. W., Joung, D. J., Redmond, M. C. & Kessler, J. D. Light rare earth element depletion during Deepwater Horizon blowout methanotrophy. *Sci. Rep.* **7**, 10389 (2017).
15. Chan, E. W. et al. Investigations of aerobic methane oxidation in two marine seep environments: part 1—chemical kinetics. *JGR Oceans* **124**, 8852–8868 (2019).
16. Hornibrook, E. R. C., Bowes, H. L., Culbert, A. & Gallego-Sala, A. V. Methanotrophy potential versus methane supply by pore water diffusion in peatlands. *Biogeosciences* **6**, 1491–1504 (2009).
17. Looman, A., Maher, D. T. & Santos, I. R. Carbon dioxide hydrodynamics along a wetland-lake-stream-waterfall continuum (Blue Mountains, Australia). *Sci. Total Environ.* **777**, 146124 (2021).

18. Hall, R. O., Kennedy, T. A. & Rosi-Marshall, E. J. Air-water oxygen exchange in a large whitewater river: air-water O2 exchange in the Colorado River. *Limnol. Oceanogr.* **2**, 1–11 (2012).
19. Tsivoglou, E. C. & Wallace, J. R. *Characterization of Stream Reaeration Capacity*. (United States Environmental Protection Agency, 1972).
20. Raymond, P. A. et al. Scaling the gas transfer velocity and hydraulic geometry in streams and small rivers: gas transfer velocity and hydraulic geometry. *Limnol. Oceanogr.* **2**, 41–53 (2012).
21. Demars, B. O. L., Thompson, J. & Manson, J. R. Stream metabolism and the open diel oxygen method: principles, practice, and perspectives. *Limnol. Ocean Methods* **13**, 356–374 (2015).
22. Grace, M. & Imberger, M. *Stream metabolism: performing & interpreting measurements*. (2006).
23. Matsuo, T. & Yotsukura, N. *An estimation of the reaeration coefficient in natural streams by spectral analysis of the Time Series Data*. (1981).
24. Parker, G. & DeSimone, L. *Estimating rearation coefficients for low-slope streams in Massachusetts and New York, 1985-1988*. (1992).
25. Langbein, W. B. & Durum, W. H. *The Aeration Capacity of Streams*. (1967).
26. Raymond, P. A. et al. Scaling the gas transfer velocity and hydraulic geometry in streams and small rivers. *Limn. Fluids Environ.* **2**, 41–53 (2012).
27. O'Connor, D. J. & Dobbins, W. E. Mechanism of reaeration in natural streams. *T. Am. Soc. Civ. Eng.* **123**, 641–666 (1958).
28. Botter, G., Carozzani, A., Peruzzo, P. & Durighetto, N. Steps dominate gas evasion from a mountain headwater stream. *Nat. Commun.* **13**, 7803 (2022).
29. Natchimuthu, S., Wallin, M. B., Klemedtsson, L. & Bastviken, D. Spatio-temporal patterns of stream methane and carbon dioxide emissions in a hemiboreal catchment in Southwest Sweden. *Sci. Rep.* **7**, 39729 (2017).
30. Leibowitz, Z. W., Brito, L. A. F., Lima, P. V. D., Eskinazi-Sant'Anna, E. M. & Barros, N. O. Significant changes in water pCO2 caused by turbulence from waterfalls. *Limnologica* **62**, 1–4 (2017).
31. Harrison, J. A., Prairie, Y. T., Mercier-Blais, S. & Soued, C. Year-2020 global distribution and pathways of reservoir methane and carbon dioxide emissions according to the greenhouse gas from reservoirs (G-res) model. *Glob. Biogeochem. Cycles* **35**, e2020GB006888 (2021).
32. Galy-Lacaux, C. et al. Gaseous emissions and oxygen consumption in hydroelectric dams: a case study in French Guyana. *Glob. Biogeochem. Cycles* **11**, 471–483 (1997).
33. Kemenes, A., Forsberg, B. R. & Melack, J. M. CO2 emissions from a tropical hydroelectric reservoir (Balbina, Brazil). *J. Geophys. Res.* **116**, G03004 (2011).
34. De Faria, F. A. M., Jaramillo, P., Sawakuchi, H. O., Richey, J. E. & Barros, N. Estimating greenhouse gas emissions from future Amazonian hydroelectric reservoirs. *Environ. Res. Lett.* **10**, 124019 (2015).
35. Tsivoglou, E. C., Cohen, J. B., Shearer, S. D. & Godsil, P. J. Tracer measurement of stream reaeration. II. Field studies. *J. (Water Pollut. Control Fed.)* **40**, 285–305 (1968).
36. Chan, E. W. et al. Investigations of aerobic methane oxidation in two marine seep environments: Part 2—isotopic kinetics. *JGR Oceans* **124**, 8392–8399 (2019).
37. Bastviken, D., Cole, J. J., Pace, M. L. & Van De Bogert, M. C. Fates of methane from different lake habitats: connecting whole-lake budgets and CH4 emissions. *J. Geophys. Res.* **113**, 2007JG000608 (2008).
38. Maeck, A. et al. Sediment trapping by dams creates methane emission hot spots. *Environ. Sci. Technol.* **47**, 8130–8137 (2013).
39. Grasso, T. *Geology and Industrial History of the Rochester Gorge Part One*. (Rochester Public Library, 1992).
40. Kershner, B. *Secret Places Scenic Treasures of Western New York and Southern Ontario*. (Kendall/Hunt Publishing Company, 1994).
41. Wiesenburg, D. A. & Guinasso, N. L. Equilibrium solubilities of methane, carbon monoxide, and hydrogen in water and sea water. *J. Chem. Eng. Data* **24**, 356–360 (1979).
42. Du, M. et al. High resolution measurements of methane and carbon dioxide in surface waters over a natural seep reveal dynamics of dissolved phase air–sea flux. *Environ. Sci. Technol.* **48**, 10165–10173 (2014).
43. Garcia-Tigreros Kodovska, F. et al. Dissolved methane and carbon dioxide fluxes in Subarctic and Arctic regions: assessing measurement techniques and spatial gradients. *Earth Planet. Sci. Lett.* **436**, 43–55 (2016).
44. Johnson, J. E. Evaluation of a seawater equilibrator for shipboard analysis of dissolved oceanic trace gases. *Anal. Chim. Acta* **395**, 119–132 (1999).
45. Niemann, H. et al. Toxic effects of lab-grade butyl rubber stoppers on aerobic methane oxidation. *Limnol. Oceanogr. Methods* **13**, 40–52 (2015).
46. Bogard, M. J. et al. Oxic water column methanogenesis as a major component of aquatic CH4 fluxes. *Nat. Commun.* **5**, 5350 (2014).
47. Grossart, H.-P., Frindte, K., Dziallas, C., Eckert, W. & Tang, K. W. Microbial methane production in oxygenated water column of an oligotrophic lake. *Proc. Natl. Acad. Sci. USA* **108**, 19657–19661 (2011).
48. Tang, K. W., McGinnis, D. F., Frindte, K., Brüchert, V. & Grossart, H.-P. Paradox reconsidered: methane oversaturation in well-oxygenated lake waters. *Limnol. Oceanogr.* **59**, 275–284 (2014).
49. Yao, M., Henny, C. & Maresca, J. A. Freshwater bacteria release methane as a by-product of phosphorus acquisition. *Appl Environ. Microbiol* **82**, 6994–7003 (2016).
50. Magen, C. et al. A simple headspace equilibration method for measuring dissolved methane. *Limnol. Ocean Methods* **12**, 637–650 (2014).
51. Leonte, M. et al. Rapid rates of aerobic methane oxidation at the feather edge of gas hydrate stability in the waters of Hudson Canyon, US Atlantic Margin. *Geochim. et. Cosmochim. Acta* **204**, 375–387 (2017).
52. Leonte, M., Ruppel, C. D., Ruiz-Angulo, A. & Kessler, J. D. Surface methane concentrations along the mid-atlantic bight driven by aerobic subsurface production rather than seafloor gas seeps. *JGR Oceans* **125**, e2019JC015989 (2020).
53. Pack, M. A. et al. A method for measuring methane oxidation rates using low-levels of 14C-labeled methane and accelerator mass spectrometry. *Limnol. Oceanogr. Methods* **9**, 245–260 (2011).
54. Kessler, J. D. & Reeburgh, W. S. Preparation of natural methane samples for stable isotope and radiocarbon analysis. *Limnol. Oceanogr. Methods* **3**, 408–418 (2005).
55. Sparrow, K. J. & Kessler, J. D. Efficient collection and preparation of methane from low concentration waters for natural abundance radiocarbon analysis. *Limnol. Oceanogr. Methods* **15**, 601–617 (2017).
56. USGS. U.S. Geological Survey National Water Information System data available on the World Wide Web (USGS Water Data for the Nation, 2023).

Acknowledgements

This research was funded by grants to J.K. from NSF (OCE-2023514, OCE-1634871, and OCE-2241873) and to R.R. for the University of Rochester Research and Innovation Grant. The authors thank Katherine Gregory, Madeline Every, Sydney Louden, and Jesse Dugan for scientific assistance throughout this study. The authors also acknowledge Rory Cottrell for helpful guidance on site selection during this study and Carolyn Ruppel for help creating Fig. 2.

Author contributions

R.R. and J.K. designed experiments relevant to waterfalls. A.F. and J.K. designed experiments relevant to methane oxidation. All authors contributed to data collection, analysis, and interpretation. All authors

contributed to manuscript writing and editing and gave final approval for publication.

Competing interests
The authors declare no competing interests.

Additional information
Supplementary information The online version contains supplementary material available at https://doi.org/10.1038/s43247-025-02060-3.

Correspondence and requests for materials should be addressed to Rebecca L. Rust or John D. Kessler.

Peer review information *Communications Earth & Environment* thanks Bridget Deemer and the other, anonymous, reviewer(s) for their contribution to the peer review of this work. Primary Handling Editors: Alice Drinkwater, Aliénor Lavergne. A peer review file is available.